



LAWRENCE
LIVERMORE
NATIONAL
LABORATORY

LLNL-TR-640046

Development of the CD Symcap platform to study gas-shell mix in implosions at the National Ignition Facility

D. T. Casey, V. A. Smalyuk, R. E. Tipton, J. E. Pino, G. P. Grim, B. A. Remington, D. P. Rowley, S. V. Weber, M. Barrios, R. Benedetti, D. L. Bleuel, E. J. Bond, D. K. Bradley, J. A. Caggiano, D. A. Callahan, C. J. Cerjan, K. C. Chen, D. H. Edgell, M. J. Edwards, D. Fittinghoff, J. A. Frenje, M. Gatu-Johnson, V. Y. Glebov, S. Glenn, N. Guler, S. W. Haan, A. Hamza, R. Hatarik, H. W. Herrmann, D. Hoover, W. W. Hsing, N. Izumi, P. Kervin, S. Khan, J. D. Kilkenny, J. Kline, J. Knauer, G. Kyrala, O. L. Landen, T. Ma, A. G. MacPhee, J. M. McNaney, M. Mintz, A. Moore, A. Nikroo, A. Pak, T. Parham, R. Petrasso, H. G. Rinderknecht, D. B. Sayre, M. Schneider, W. Stoeffl, R. Tommasini, R. P. Town, K. Widman, D. C. Wilson, C. B. Yeamans

July 1, 2013

Disclaimer

This document was prepared as an account of work sponsored by an agency of the United States government. Neither the United States government nor Lawrence Livermore National Security, LLC, nor any of their employees makes any warranty, expressed or implied, or assumes any legal liability or responsibility for the accuracy, completeness, or usefulness of any information, apparatus, product, or process disclosed, or represents that its use would not infringe privately owned rights. Reference herein to any specific commercial product, process, or service by trade name, trademark, manufacturer, or otherwise does not necessarily constitute or imply its endorsement, recommendation, or favoring by the United States government or Lawrence Livermore National Security, LLC. The views and opinions of authors expressed herein do not necessarily state or reflect those of the United States government or Lawrence Livermore National Security, LLC, and shall not be used for advertising or product endorsement purposes.

This work performed under the auspices of the U.S. Department of Energy by Lawrence Livermore National Laboratory under Contract DE-AC52-07NA27344.

Development of the CD Symcap platform to study gas-shell mix in implosions at the National Ignition Facility

D. T. Casey,¹ V. A. Smalyuk,¹ R. E. Tipton,¹ J. E. Pino,¹ G. P. Grim,² B. A. Remington,¹ D. P. Rowley,¹ S. V. Weber,¹ M. Barrios,¹ L. R. Benedetti,¹ D. L. Bleuel,¹ E. J. Bond,¹ D. K. Bradley,¹ J. A. Caggiano,¹ D. A. Callahan,¹ C. J. Cerjan,¹ K. C. Chen,⁵ D. H. Edgell,³ M. J. Edwards,¹ D. Fittinghoff,¹ J. A. Frenje,⁴ M. Gatou-Johnson,⁴ V. Y. Glebov,³ S. Glenn,¹ N. Guler,² S. W. Haan,¹ A. Hamza,¹ R. Hatarik,¹ H. W. Herrmann,² D. Hoover,⁵ W. W. Hsing,¹ N. Izumi,¹ P. Kervin,¹ S. Khan,¹ J. D. Kilkenny,⁵ J. Kline,² J. Knauer,³ G. Kyrala,² O. L. Landen,¹ T. Ma,¹ A. G. MacPhee,¹ J. M. McNaney,¹ M. Mintz,¹ A. Moore,⁶ A. Nikroo,⁵ A. Pak,¹ T. Parham,¹ R. Petrasso,⁴ H. G. Rinderknecht,⁴ D. B. Sayre,¹ M. Schneider,¹ W. Stoeffl,¹ R. Tommasini,¹ R. P. Town,¹ K. Widmann,¹ D. C. Wilson,² and C. B. Yeamans¹

1) Lawrence Livermore National Laboratory, Livermore, CA 94550

2) Los Alamos National Laboratory, Los Alamos, NM 87545

3) Laboratory for Laser Energetics, University of Rochester, Rochester, NY 14623

4) Massachusetts Institute of Technology, Cambridge, MA 02139

5) General Atomics, San Diego, CA 92121

6) AWE Aldermaston, Reading, Berkshire, RG7 4PR, United Kingdom.

Surrogate implosions play an important role at the National Ignition Facility (NIF) for isolating aspects of the complex physical processes associated with fully integrated ignition experiments. The newly developed CD Symcap platform has been designed to study gas-shell mix in indirectly driven, pure T₂-gas filled CH-shell implosions equipped with 4 μm thick CD layers. This configuration provides a direct nuclear signature of mix as the DT yield (above a characterized D contamination background) is produced by D from the CD layer in the shell, mixing into the T-gas core. The CD layer can be placed at different locations within the CH shell to probe the depth and extent of mix. CD layers placed flush with the gas-shell interface and recessed to up to 8 μm have shown that most of the mix occurs at the inner-shell surface. In addition, time-gated x-ray images of the hotspot show large brightly-radiating objects traversing through the hotspot around bang-time, which are likely chunks of CH/CD plastic. This platform is a powerful new capability at the NIF for understanding mix, one of the key performance issues for ignition experiments.

I. Introduction

Hydrodynamic instabilities that grow during Inertial confinement fusion (ICF) experiments, performed at the National Ignition Facility (NIF),^{1, 2, 3} inject cold and high-Z material into the hotspot that can quench thermonuclear burn.⁴ Turbulent instability growth during the deceleration phase of the implosion, also called mix, is one of the key performance issues for cryogenic ignition experiments.^{5, 6} It is therefore necessary to properly design targets that are robust to the deleterious effects of mix.

During the course of the National Ignition Campaign,⁷ experiments showed that current ignition designs were susceptible to an unacceptable amount of mix. For example, measurements of Ge doped capsule implosions have demonstrated that ablator material mixes through the ice layer and into the hotspot in cryogenic implosions.⁸ Also, measurements of X-ray yields relative to the neutron yields, in cryogenic DT experiments, have been used to quantify the amount of ablator material that mixes into the hotspot. These data have shown that inferred mix mass has a strong inverse correlation with the overall yield.⁹ To help understand these results, focused experimental campaigns are now underway to study and test calculations of both acceleration phase instability growth using x-ray radiography of pre-imposed perturbations¹⁰ and deceleration phase instability growth by observing nuclear signatures of gas-shell atomic mix.

In particular, a focused experimental platform called the “CD Symcap” platform was designed and deployed to test mix modeling used in simulating experiments on the NIF, as first reported in ref. ¹¹. This paper follows up with additional results from experiments, analysis, and calculations from the CD

Symcap campaign. The platform uses the same hohlraum, drive, and ablator as ignition targets but rather than a cryogenic DT ice layer, the “Symcap” capsule uses a surrogate plastic payload, in addition to the typical Si-doped plastic ablator. Originally designed to measure and tune hot-spot symmetry,¹² the Symcap platform has here been extended to study gas shell mix by inserting a thin layer of deuterated plastic and filling the capsule with extremely pure tritium gas (<0.15 mole % deuterium). The CD Symcap experiments are designed to directly probe atomic-scale fuel-shell mix through observations of the DT yield that occurs from tritium and deuterium, which were initially separated, but have become turbulently mixed and heated. This technique has been used successfully before in direct drive laser experiments that used deuterated plastic layers (CD) with tritium filled¹³ and helium-3 filled capsules^{14, 15, 16} at the OMEGA laser facility.¹⁷ The present CD Symcap experiments are nonetheless unique, as they represent the first time this technique has been used in indirect drive and at the full energy scale available at the NIF.⁵ In addition, these experiments are performed using actual ignition drives and targets (with surrogate plastic instead of ice) to be as relevant as possible to ignition platforms.

The experimental target design is illustrated in Figure 1. The deuterated plastic layer is either placed flush with or recessed by up to 8 μm from the gas-shell interface. The CD Symcap target is of the so-called “Rev5” ignition target design.⁴ The Au hohlraum dimensions are 5.75 mm inner diameter by 9.43 mm tall (inside) with a 3.373 mm in diameter laser entrance hole. The hohlraum is filled with 0.96 ± 0.01 mg/cm³ of helium gas to tamp the Au-plasma ablated from the hohlraum wall to improve irradiation symmetry, while also controlling laser plasma instabilities and cross-beam energy transfer.^{4, 18} The entire target assembly including capsule and hohlraum is maintained at 32 K using the

thermo-mechanical package designed and used for cryogenic DT experiments.⁶

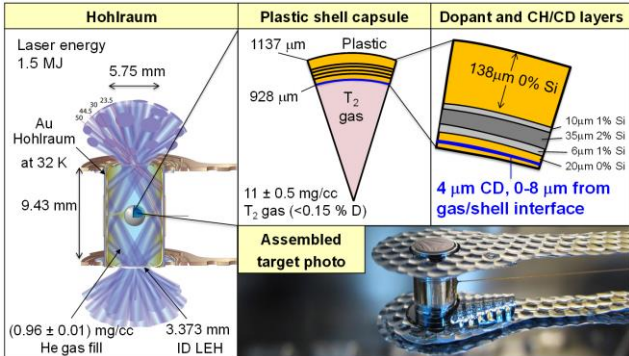


Figure 1: Schematic of indirectly driven CD Symcap target. Lasers irradiate the inside of a Au hohlräum, which produces x-rays that drive the capsule imploding inward. The capsules are filled with pure tritium gas and the shell contains deuterated plastic layers at different distances from the gas-shell interface. The DT neutron yield of the imploded capsule is a direct measure of atomic scale fuel-shell mix. Included also in the bottom right panel is a photograph of the assembled target used in shot N121119.

The capsule is nominally 1137 μm in radius with a total shell thickness of 209 μm . To shield the inner payload (usually DT ice but plastic in Symcaps) from the x-ray drive, and thereby reduce density discontinuities and instabilities,¹⁹ the plastic ablator is doped with three layers of graded Si (thicknesses and dopant concentration described in Figure 1). The inner plastic layer contains a mass-equivalent payload of plastic to hydrodynamically match a typical cryogenic ice layer, momentum balanced to achieve similar implosion velocity. We use the density of CH at 1.06 g/cc (at 32 K) and the solid DT density of 0.255 g/cc (the small density difference of doped CD layers in the payload are neglected). Figure 2a shows a capsule diagram of an ignition target (shot N111215) while Figure 2b shows a diagram of a symcap target.

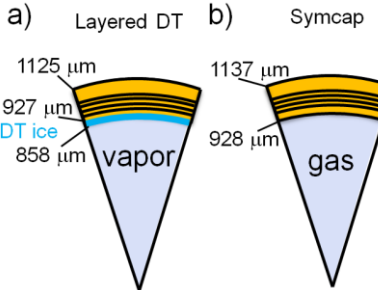


Figure 2: a) Diagram of a typical layered DT ignition target. The Si dopant follows the thickness and amounts outlined in Figure 1. b) Diagram of a plastic shell symcap target.

The CD layer is 4 μm thick and placed flush to the gas-shell interface or recessed up to 8 μm . Figure 3 shows a backscatter scanning electron microscope (SEM) image²⁰ of two CD Symcap capsules, one with the CD layer flush on the gas-shell interface (a) and one with the CD layer recessed 8 μm (b). These SEM images are of the first few layers near the gas-shell interface.

They were taken after destroying the targets by fracturing the capsule and taking an image slice through the capsule wall but are representative of the capsules used in these experiments, as they were manufactured using the same techniques. Clear discontinuities are observed between CH, CH doped with Si, and CD layers due to differences in density and polymer-production techniques of the different plastic layers.

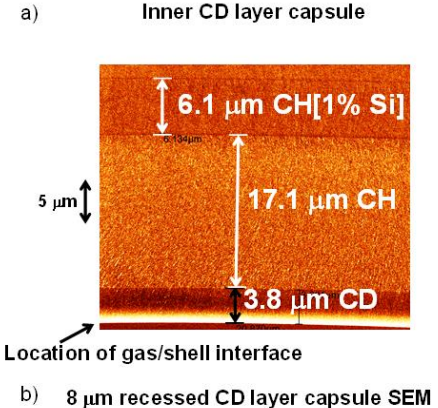


Figure 3: a) Backscatter scanning electron microscope (SEM) image of a CD Symcap capsule with a 3.8 μm CD layer flush against the gas-shell interface, followed by 17.1 μm of undoped CH, and then followed by 1 % Si doped CH. More layers follow beyond the image field of view, as illustrated in Figure 1. b) SEM image of a CD Symcap capsule with the CD layer recessed by 8.4 μm from the gas-shell interface with undoped CH. The CD layer is followed by another 8.0 μm of undoped CH, and then 6.1 μm of CH doped with 1% Si. More layers follow beyond the image field of view, as illustrated in Figure 1.

The capsule is filled with 11.1 ± 0.5 mg/cc of purified tritium gas corresponding to 4.0 atm at 32 K. An upper limit of 0.15 atom-% residual deuterium contamination in the gas was determined by first filling the capsule, then retracting the gas from the fill system, and subjecting the sample to mass-spectrometry. Furthermore, several contamination shots were performed without CD layers to show DT yield from residual D in the gas (as will be discussed in more detail later) and the results were consistent with D levels measured in the gas.

The laser drive was matched to cryogenic DT shot N111215, which utilized a 1.5 MJ laser pulse and a 434 TW peak power as shown in Figure 4. To help control hotspot symmetry, 145 TW was incident on the 23.5° and 30° or inner cone laser beams and 289 TW on the 44.5° and 50° or outer cone beams illustrated in Figure 1. As an additional control of hotspot symmetry,²¹ the inner 23.5° beams were operated at 8.1 Å larger wavelength and the 30° inner beams were operated at 6.6 Å larger wavelength

than the outer cone beams. The hohlraum radiation temperature produced by the laser drive, as inferred by the Dante diagnostic, is also shown in Figure 4. The peak radiation temperature was consistently 303 ± 4 eV for all shots in the campaign. As indicated on the figure, the x-ray bang-time (defined as peak x-ray self-emission brightness) occurred consistently ~ 1.5 ns after the end of the laser drive at 22.5 ns.

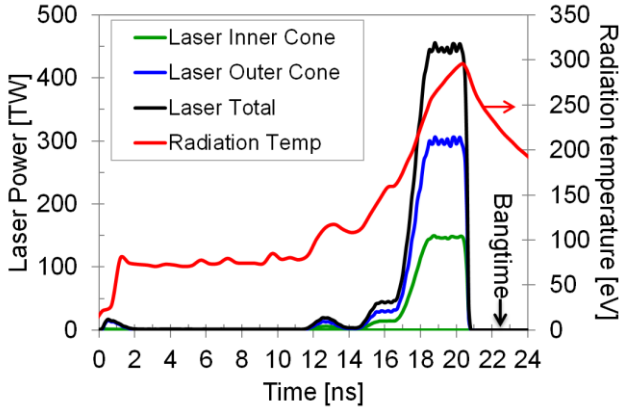


Figure 4: Measured laser pulse used to drive shot N130512 at 436 TW peak power, plotted as total power as a function of time. All shots described here used the same laser pulse with excellent repeatability. Also shown is the measured hohlraum radiation temperature in eV, as determined from the DANTE diagnostic. The peak radiation temperature was 303 eV, and the implosion x-ray bang-time was at 22.5 ns.

Despite careful matching of drive and target conditions to cryogenic DT experiments, there are important differences in CD Symcaps that must be considered in the context of mix. First, the imploded Symcap convergence ratios (R_0/R) are ~ 15 , roughly a factor of 2 lower than typical cryogenic DT implosions and therefore also achieve lower shell density at stagnation. Mix is very sensitive to convergence, which likely decreases the instability growth when compared to a cryogenic DT implosion. Second, the Atwood number at the gas-shell interface may be higher, due to the larger density plastic payload (compared to DT ice), which likely leads to higher deceleration instability growth. In addition, ablator plastic must mix through the dense DT shell into the hotspot in order to degrade the yield in cryogenic DT implosions that do not achieve propagating shell burn. Figure 5 shows the simulated density and pressure profiles for ignition targets and symcap targets compared at peak acceleration (right panel) and peak velocity (left panel). Regardless of these differences, the data obtained from CD Symcaps provides direct and unambiguous measures of gas-shell atomic mix that are essential for testing and developing the mix modeling used to design and understand ignition experiments.

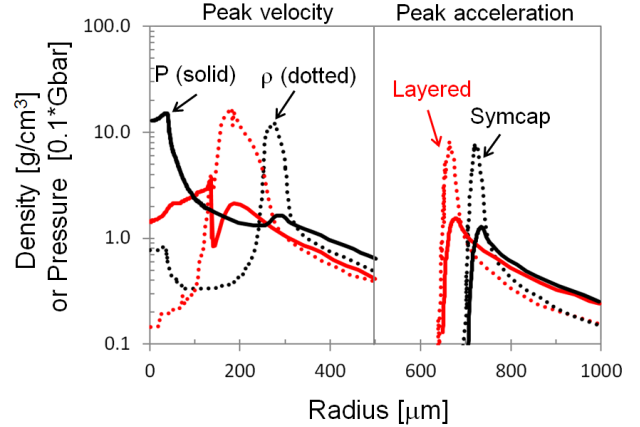


Figure 5: Simulations comparing symcap and layered target densities (dotted) and pressures (solid) produced with the radiation hydrodynamics code ARES²² at peak acceleration (right panel) and peak velocity (left panel).

II. Modeling CD Symcap experiments

A. 1D hydrodynamic simulations using CALE-KL

The experiments described herein were designed using the arbitrary Lagrangian–Eulerian hydrodynamic code CALE,^{23,24} which numerically solves the fluid equations to simulate the implosion hydrodynamics. Coupled to the KL turbulent mix model,²⁴ CALE-KL predicts atomic scale mix in CD Symcap implosions. The KL model describes the turbulence scale size and kinetic energy from multi-mode nonlinear Rayleigh-Taylor (RT) and Richtmyer-Meshkov (RM) instabilities in ICF implosions. With the constraints developed in the model, one free parameter L_0 remains, which is the initial turbulence spatial scale length. Figure 6 shows an example calculation using CALE-KL for a DT filled Symcap, designed to obtain the high neutron yield required to employ the full nuclear diagnostic suite (useful for pR and nuclear gamma bang-time measurements). It is worth noting that the DT Symcap (illustrated in Figure 6a) is predicted to have similar overall hydrodynamic behavior as TT filled Symcap capsules, both with and without CD layers, because it was filled with the same initial fuel particle (fully ionized ion + electron) density. The predicted gas and shell density profiles at bang-time are shown in Figure 6b (calculated using 1D CALE-KL with an $L_0 = 2000$ nm). The value of $L_0 = 2000$ nm is what allows the 1D calculation to best match the overall performance as this approximates the growth of asymmetries of all modes (since the 1D calculation cannot explicitly resolve asymmetry). This value is of the same order of the capsule outer surface roughness RMS over all modes. The KL model allows the CH and DT to mix together. As the CH mixes into the hotspot, it radiates and cools the implosion, which degrades the core hotspot performance by effectively shrinking the burning volume. This is evident as the simulated burn profile ends where CH is mixing into the hotspot. This is in contrast to CD Symcaps, where the DT neutron yield probes the atomic scale mix of T and D in this mixing region. Note also that the TT yield in CD Symcaps simultaneously probes the hotspot since the yield is degraded by both atomic-scale mix and larger-scale chunks and spikes of shell material. It is also worth noting that these 1D simulations over estimate the amount atomic scale mix in these experiments,

motivating higher dimensional calculations to explicitly resolve lower mode growth.

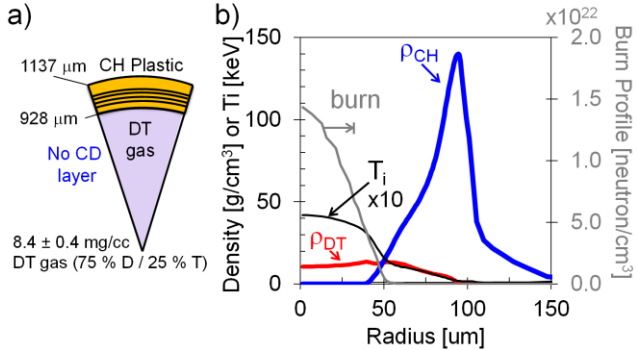


Figure 6: a) Diagram of a plastic DT gas-filled CH-capsule Symcap implosion designed for high yield to employ the full suite of neutron diagnostics. This target is similar to the CD Symcap described in Figure 1, except that the gas is DT and the capsule does not have a CD layer. b) 1D simulated density profiles at bang-time for the CH shell (blue curve) and DT gas (red curve) of a Symcap implosion. These profiles were calculated using the hydrodynamics code CALE-KL. Coupled with the turbulent diffusion model KL,²⁴ these simulations include predictions of the mix of the CH ablator material with the DT gas material. The simulated burn profile is shown in grey, which gives the neutron density (neutrons/cm³) produced from the D+T → $\alpha+n$ reaction. The simulated ion temperature (T_i) is also shown multiplied by 10 to fit on scale (black curve).

B. 2D hydrodynamic simulations using ARES-KL

The radiation hydrodynamics code ARES²² was used to perform 2D simulations with an angular resolution of 1/8 degree.²⁵ These simulations capture low- to mid-mode (Legendre modes up to $l=100$) hydrodynamic instabilities by initializing the problem with an imposed surface roughness; fill-tube, tent, and drive asymmetries are not included. High-mode turbulence leading to atomic mix is captured using the KL mix model.

Figure 7a shows the 2D simulated ion temperature (T_i) and density profiles for a 3× nominal capsule surface roughness (described later as the surface roughness required to match the

platform performance, determined by the TT neutron yield).

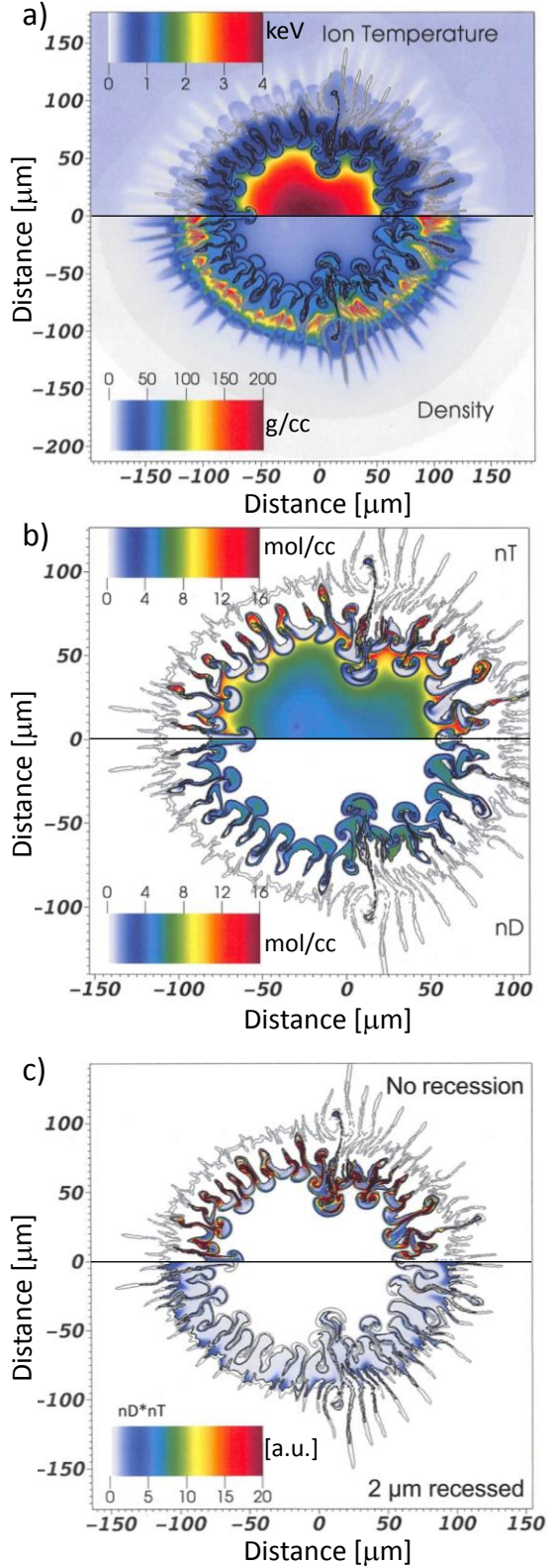


Figure 7: a) The 2D simulated Ti (top section) and density (bottom section) distribution using ARES with the KL mix model. The black curve shows the gas-shell and CD/CH boundaries of the CD layer, where initially the CD layer was placed at the gas/shell interface. Fingers (RT spikes) move into the hot spot from growth seeded by outer capsule surface defects. This simulation used $3\times$ the Rev5 surface requirement,²⁶ which produced good agreement with the core TT neutron yield. b) Simulated tritium density (top section) and the deuterium density (bottom section) in moles/cc for an inner surface CD layer implosion. c) Product of the simulated deuterium number density (n_D) and tritium number density (n_T) for an inner surface CD layer (top section) and a $2\ \mu\text{m}$ recessed CD layer (bottom section). The density product is the mix region where DT yield is produced in a CD Symcap (weighted toward the center by the temperature gradient shown in (a)). Fig. 5c was reprinted with permission from V. A. Smalyuk et. al., Physical Review Letters 112, 025002 (2014). Copyright 2014 American Physical Society.

Figure 7b shows the deuterium and tritium ion densities. The tritium density (top section) is highest in the outer part of the core, since the pressure is slowly varying at stagnation and the temperature is decreasing quickly with radius and $P\sim 2nT$ (Figure 7a). The tritium density is highest where tritium-filled bubbles penetrate into the shell and are being compressed by spherical convergence effects. The deuterium density (bottom section) indicates the location of the CD layer including the mixed region where D and T can fuse. This figure indicates that D mixes into the core on the tips of RT fingers (spikes). This is better illustrated in Figure 7c, showing the product of the deuterium and tritium densities. The DT yield is produced on the outside of the central core in an hollow-spherical mix region. Due to the strong radial temperature gradient and the temperature dependence of the DT reactivity, the DT yield is weighted toward the inner side of the mix region.

III. Observed data from CD Symcaps

Table 1 – Summary of observables from several TT filled CD Symcaps. The TT yield is a metric of overall performance, whereas the DT yield is a metric of gas-shell mix.

Shot Number	N120904	N121119	N121125	N130510	N130317	N130315	N130512	N130612	N130614
CD layer location	CH control	CH control	Inner CD layer	Inner CD layer	1um offset	2um offset	2um offset	4um offset	8um offset
T _i (keV) [ntof]	3.4 ± 0.4	3.5 ± 0.1	2.1 ± 0.1	2.2 ± 0.1	2.1 ± 0.2	2.2 ± 0.1	2.6 ± 0.1	2.9 ± 0.1	3.4 ± 0.1
DT Yield x10 ¹³	0.41 ± 0.02	0.40 ± 0.01	2.5 ± 0.07	2.4 ± 0.08	2.0 ± 0.06	0.88 ± 0.03	1.3 ± 0.04	0.72 ± 0.03	0.67 ± 0.03
TT Yield x10 ¹³	2.2 ± 0.2	2.1 ± 0.2	2.2 ± 0.2	1.9 ± 0.2	2.7 ± 0.3	2.3 ± 0.2	3.4 ± 0.3	2.3 ± 0.2	2.4 ± 0.2
DSR (%)	1.0 ± 0.1	1.1 ± 0.1	1.0 ± 0.1	1.1 ± 0.1	1.3 ± 0.3	1.1 ± 0.1	1.2 ± 0.1	0.7 ± 0.3	0.7 ± 0.3
X Bang-time (ns)	22.58 ± 0.07	22.55 ± 0.07	22.50 ± 0.05	22.53 ± 0.02	22.55 ± 0.04	22.53 ± 0.03	22.53 ± 0.02	22.54 ± 0.01	22.56 ± 0.01
X-ray burn (ps)	291 ± 60	267 ± 36	307 ± 12	312 ± 30	309 ± 11	316 ± 9	320 ± 30	320 ± 15	325 ± 15
X-ray P ₀ (μm)	56 ± 10	60 ± 4	60.2 ± 4	55 ± 2	59 ± 3	53 ± 4	59 ± 2	63 ± 5	64 ± 5
X-ray P ₂ /P ₀ (%)	10 ± 1.4	12 ± 0.7	13 ± 0.7	16 ± 1.1	1.3 ± 1.9	8.4 ± 2.6	15 ± 2.4	24 ± 4	23 ± 6
X-ray M ₀ (μm)	59 ± 4	69 ± 3		57 ± 8	65 ± 5	65 ± 6	58 ± 4	60 ± 3	
X-ray M ₄ /M ₀ (%)	1.5 ± 5.2	2.1 ± 3.2		1.9 ± 0.9	4.7 ± 3.6	4 ± 4	2.8 ± 0.3		3 ± 2

A. Neutron observations, TT yield, DT yield, and ion temperature

In a T₂ gas-filled CD Symcap implosion, the DT fusion yield is a direct measure of the D mixing into to the hot tritium core (when ignoring the trace D impurity in the tritium gas). Simultaneously, the TT fusion yield probes conditions of the hot core and is sensitive to the overall implosion performance. Quantitatively, the fusion yield of two reactants, 1 and 2 (1 and 2 could be DT or TT), can be described generally by:

$$Y_{12} = \int \frac{n_1(\vec{r}, t) n_2(\vec{r}, t)}{1 + \delta_{12}} \langle \sigma v \rangle_{12} d\vec{r} dt, \quad (1)$$

where n_1 and n_2 are the ion densities, $\langle \sigma v \rangle$ is the fusion reactivity, and δ_{12} is the Kronecker delta that accounts for double counting of identical reactants.²⁷ The fusion reactivity is the Maxwellian averaged product of the cross-section and relative ion velocity, and requires accurate knowledge of the DT and TT fusion reaction cross-sections.²⁸ Fortunately, the DT cross-section has been studied extensively at energies relevant to the experiments discussed here and is generally well known.^{28, 29} Less data is available for the TT fusion cross-section.²⁸ It is, nevertheless, well constrained for the present work (to better than 14% at the relevant energies) by two data sets obtained by Serov et al.³⁰ and Brown et al.³¹

Using Eq. 1, the DT neutron yield can be approximately evaluated in the mix region by:

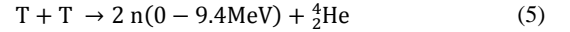
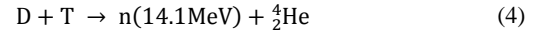
$$Y_{DT} \approx n_D n_T \langle \sigma v \rangle_{DT} V_{mix} \tau_{mix} + Y_{DT-cont}, \quad (2)$$

where n_D and n_T are the average particle densities of D and T, V_{mix} is the burn volume of the mix region, τ_{mix} is the burn duration in the mix region and $Y_{DT-cont}$ is the yield from residual deuterium contamination in the tritium gas. A burn weighted metric of mix-mass in the hot spot is then related to the product of $\sim n_D V_{mix}$. Correspondingly, the TT reaction yield from the core (or hotspot) can be approximately evaluated by:

$$Y_{TT-rx} \approx \frac{1}{2} n_{T-core}^2 \langle \sigma v \rangle_{TT} V_{core} \tau_{core}, \quad (3)$$

where now the τ_{core} and V_{core} are evaluated for the core.

The DT and TT fusion reactions both produce diagnostic neutrons, which are the basis for the measurement of mix in the CD Symcap experiments, as described by:



Note that unless otherwise specified, all discussion herein of the TT yield refers to the TT neutron yield, which is two times the TT reaction yield. The exact details of the TT neutron spectrum are sensitive to the interactions between the emitted particles in the final state.³² Knowledge of the TT neutron spectrum is important because it is required to connect observations, which are typically limited to a finite energy range due to detector cutoffs to Eqs. 2 and 3. Calculating the TT neutron spectrum *ab initio* is challenging and work in this field is ongoing.³³ However, the TT neutron spectrum has been measured in a variety of accelerator and ICF experiments³⁴⁻³⁸ and various models have been developed. In fact, the TT spectrum generated from these NIF experiments represents the highest quality data produced to date, and has most recently been interpreted through R-matrix

modeling.³⁸ Furthermore, the error in the measured TT yield is minimized as the TT neutron yield is obtained with six independent diagnostics, including three different nuclear techniques such as: foil activation,³⁹ neutron time of flight (nTOF),^{40, 41} and the magnetic recoil spectrometer (MRS).⁴²⁻⁴⁴ An estimate of the systematic error in the measured TT neutron yield based on the comparisons of different models, diagnostics, and analysis techniques is ~10 %.

An example set of measured neutron spectra are shown in Figure 8. These are deconvolved spectra obtained from the nTOF-SP diagnostic, located ~18 m from the implosion.⁴⁵ The data were obtained from a pure tritium control shot without a CD layer (red), and from an identical implosion with a target with a CD layer flush on the gas-shell interface (blue). The DT yield is six times higher for the implosion with the CD layer, while the TT yield is nominally the same (see Table 1), demonstrating fuel-shell instabilities are mixing deuterium into the hotspot.

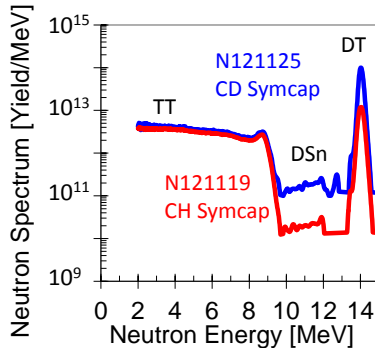


Figure 8: Neutron spectra measured with the SpecSP neutron time of flight detector positioned 18 m away from the implosions for a TT control capsule without a CD layer (N121119) and a CD Symcap with a CD layer flush with gas-shell interface (N121125). Immediately apparent is the stronger DT peak in the CD Symcap, which is caused by mix. Also shown are the down-scattered neutron (DSn) spectra, which are proportional to the product of the implosion pR and the DT yield. Note that the region between 12-13 MeV, is poorly described due to a deconvolution artifact from the strong 14 MeV peak feature and is currently being improved. The TT neutrons are apparent in the region below ~9.5 MeV. The nearly overlapping TT-spectra show that these two implosions had very similar core performance.

The measured TT neutron yield for two T_2 -CH Symcap control shots, which were tritium filled capsules with CH shells without CD layers, are shown by the black data points in Figure 9a. The TT neutron yield for several CD Symcaps, as a function of the CD-layer depth from the gas-shell interface, is also shown. The TT yield is on average 2.2×10^{13} and reproducible to 20% (standard deviation) within all shots. The two highest TT neutron yield implosions used thinner capsule support tents, 45 nm versus 110 nm, and had relatively clean capsule surfaces compared to the average. This may imply that outer capsule surface perturbations have a significant impact on the overall implosion performance, a subject of current study.

Also shown in Figure 9a are 2D ARES simulations with KL (described earlier in Figure 7), where the outer surface roughness was scaled to match the TT neutron yield. Clean calculations

over predict the TT yield by a factor of 2-3. A good match was found using a factor of 3 multiplier on the Rev5 surface roughness specification²⁶ (which was about 2 – 5 times the measured surface roughness). The overall TT performance is insensitive to small values of L_0 (described later to match other observables) because low-mode instabilities dominate the yield degradation of TT coming from the hot core. In addition, the TT yield predicted with ARES is insensitive to the presence or changes in recession depth of the CD layer, which is in agreement with the observations. This is because the difference in CD density (1.14 g/cc at 32 K) compared with CH (1.06 g/cc at 32 K) is minimal, allowing for very similar hydrodynamics.

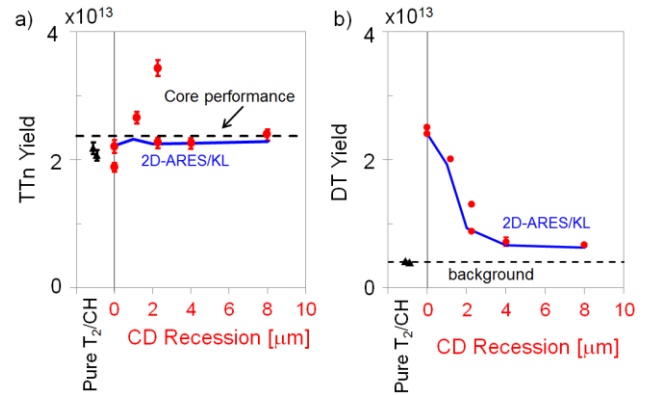


Figure 9: a) Measured TT neutron yield for two tritium-filled CH Symcaps (black), which characterize the D contamination background for several CD Symcaps (red). The CD Symcap TT yield is plotted as a function of the recession depth of the CD layer from the gas-shell interface. As expected, no trend with recession depth is observed. Simulated ARES yields are also shown as the solid blue curve. The surface roughness in the simulations was adjusted to match the TT yield. b) Measured DT yield for two TT CH Symcaps and several CD Symcaps. The DT yield from the TT CH Symcaps characterizes the background from D contamination (<0.15% D) in the tritium and the core performance, while the DT yield from the CD Symcaps is from mix. Data is reprinted with permission from V. A. Smalyuk et. al., Physical Review Letters 112, 025002 (2014). Copyright 2014 American Physical Society.

The DT neutron yield is shown in Figure 9b for two control TT Symcaps (contamination D only, no CD layer), and several CD Symcaps. The DT yield for the CD Symcaps is plotted as a function of the recession depth of the CD layer from the gas-shell interface. The DT yield drops with increasing recession distance because the mix yield is dominated by material mixing in from the inner part of the shell. Although not shown, a 75/25 DT Symcap was also imploded and produced $6.8 \pm 0.2 \times 10^{14}$ DT neutrons with a down-scattered neutron ratio (related to areal density and defined as neutron yield 10-12 MeV over 13-15 MeV)^{44, 46, 47} of $1.1 \pm 0.1\%$. Figure 10a provides the DT neutron to TT neutron yield ratio (DT/TT), a metric that is related to mix. Note that the background DT neutron yield from residual contamination has not been subtracted but is indicated on the graph. Interestingly, even though there is some scatter in the TT and DT neutron yield for identical shot repeats (at 0 and 2 μ m recession), the DT/TT ratio remains very repeatable.

In the 2D ARES-KL simulations, shown in Figure 9b, the assumed surface roughness was adjusted to 2-6 times larger than

the measured value to match the TT yield and the L_0 in the KL model was adjusted to 0.1 nm to the match DT yield for the capsule with the CD layer on the gas-shell interface (zero recession depth). With those two parameters fixed, the ARES-KL calculations provide a reasonable match to the measured DT neutron yield as the CD layer recession depth is varied.

T_i is determined from the Doppler broadened DT neutron peak, which is measured with the nTOF suite^{40, 41} and MRS diagnostics,⁴² and represents a burn-averaged DT- T_i . The determined T_i for a DT Symcap filled to 75% deuterium and 25% tritium is shown in Figure 10b along with two TT Symcaps, where the DT neutrons are produced by contamination D in the core gas. The TT Symcaps are in excellent agreement with the core temperature of the DT Symcap indicating similar burn conditions at ~ 3.5 keV. Figure 10b also shows the T_i measured from the mix region from several CD Symcaps. The T_i for the CD Symcap at the gas-shell interface is ~ 2 keV, much lower than the core temperature, because CD-shell mix from deuterium enters the outside, cooler, part of the core. T_i increases from ~ 2 keV and approaches the core temperature of ~ 3.5 keV, with increasing depth of recession, because the relative contribution of the cooler mix yield decreases to that of the D contamination yield in the central core. A summary of all yields and T_i is provided in Table 1.

Figure 10b shows T_i predictions made by ARES for the CD Symcap implosions, as a function of the depth of recession. ARES captures the T_i of the CD Symcaps at all recessions well, indicating that the radial location and extent of the mix seems to be well understood (because temperature is a function of radius as noted in Figure 6).

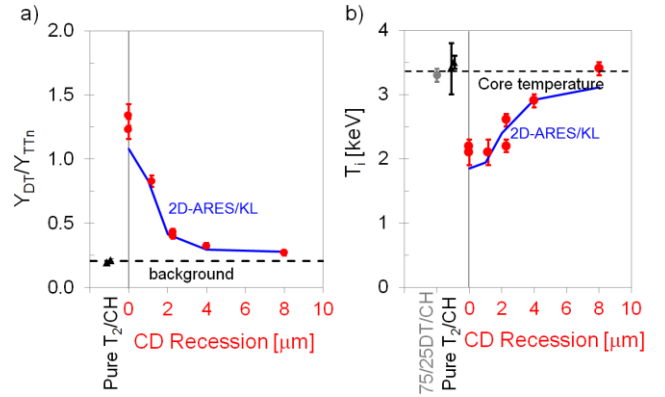


Figure 10: a) Measured TT to DT neutron yield ratio for CD Symcaps, as a function of the recession depth for the CD layer from the gas-shell interface. The DT/TT yield ratio, a measure of the atomic mix in the core, decreases as a function of recession depth, demonstrating sensitivity of the platform to gas-shell mix. b) Measured T_i determined by the Doppler width of the DT neutron peak for a DT Symcap, two pure TT Symcaps (DT neutrons are produced with D contamination in the T_2 gas), and several CD Symcaps. The T_i of the DT and TT Symcaps characterize the burn averaged core temperature. The CD Symcaps are plotted as a function of the recession depth of the CD layer from the gas-shell interface. As the recession depth increases, T_i approaches the core value because fewer neutrons are produced in the cooler mix region. Simulated ARES ion temperatures are in good agreement with observations. Data is reprinted with permission from V. A. Smalyuk et. al., Physical Review Letters 112, 025002 (2014). Copyright 2014 American Physical Society.

An approximate estimate of the burn-averaged mix mass has been made from the data by combining Eq. 2 and Eq. 3. This is accomplished by assuming an isobaric relationship between the core and burning mix regions and recasting Eq. 3 into the form for the TT neutron yield (note that there are two neutrons per TT reaction) as a function of the plasma pressure P :

$$Y_{TT-n} \approx \left(\frac{P}{2 T_{core}} \right)^2 \langle \sigma v \rangle_{TT} V_{core} \tau_{core}. \quad (6)$$

The TT neutron yield is then used to determine the tritium density in the mix region and substituted back into Eq. 2 and solving for $m_{CD} \sim n_D V_{mix}$. By neglecting the CD contribution to the pressure in the mix region (expected to be a fairly reasonable assumption in the burn-weighted part of the mix region),⁴⁸ the inferred mix mass takes a particularly simple form. Assuming the same CD ratio as in the pre-shot shell (1.35 D/C), evaluating constants, and solving for the mix mass leads to the following relationship:

$$m_{CD} \sim 1.2 \times 10^{-7} \frac{T_{mix}}{T_{core}} \frac{\sqrt{\tau_{core}}}{\tau_{mix}} \frac{\sqrt{\langle \sigma v \rangle_{TT-core}}}{\langle \sigma v \rangle_{DT-mix}} \frac{Y_{DT}}{\sqrt{Y_{TT}}} R^{3/2} \quad (7)$$

where the mass is in ng, reactivity $\langle \sigma v \rangle$ in cm³/s, burn duration τ in ps, yields Y_{DT} and Y_{TT} in units of 10^{13} neutrons, average core radius R in μm , and T_{mix} and T_{core} represent the temperature in the mix region and core, respectively.

Figure 11 shows the result of recasting the observations of Figure 9 and Figure 10 into inferred mass by using Eq. 7 plotted as a function of pre-shot CD recession (red points). Here, the contamination DT yield $Y_{DT\text{-bkg}}=(4.1\pm 0.1)\times 10^{12}$ has been subtracted by removing the background level (shown in Figure 9b) observed in the two TT Symcap control shots (with no CD layer). $T_{core} = 3.5 \pm 0.1$ keV was also obtained from the averaged DT temperature of these control shots and used as a characteristic core temperature in Eq. 7. τ_{mix} and τ_{core} are assumed to be the approximately equal and taken from x-ray burn width (see Table 1). V_{core} is estimated from the x-ray core-emission images.

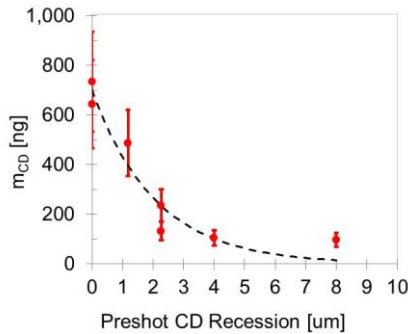


Figure 11: Inferred CD mix mass as a function of pre-shot CD recession determined using the data from Figure 9, Figure 10 and Eq. 7

The observed data show a swift drop in inferred CD mix mass, consistent with the drop in DT yield observed in Figure 9b and Figure 10a. The mixing scale length can be estimated by determining the approximate rate at which the mix mass falls as a function of pre-shot recession (ΔR), i.e. $\sim e^{-\Delta R/L}$, and then the scale length follows as $m/\nabla m = L$. However, the finite 4 μm thickness (t) of the CD layer must be considered, which results in the following correction $\sim e^{-\Delta R/L} - e^{-(\Delta R+t)/L}$, where again $m/\nabla m = L$. Shown by the black dashed curve in Figure 11, this result implies a total inferred mix mass of ~ 820 ng and a (pre-shot recession depth) mixing scale length of $\sim 2.1\mu\text{m}$.

Therefore, most of the turbulent atomic-scale mix occurs with material on the inner surface of the shell during the deceleration phase of the implosion. The gross penetration of CH into the hot spot, however, comes from the RT spike penetration (see Figure 7). The data may also be consistent with additional contributions from ablation front instabilities driven during the acceleration of the shell. This is suggested by a leveling off of the inferred mix mass at the deepest recessions. Although a relatively small component in these experiments, this may be of particular importance for cryogenic DT implosions as ablation front instabilities drive deep mix via jets that have the potential of penetrating the dense DT shell and injecting material into the hotspot. Ablation front instabilities will be the subject of future studies using higher convergence implosions, the addition of multiple spectroscopic tracers (Ge and Cu), and with further recessed and thicker CD layers.

B. Observed DD neutron yield in DT Symcaps

It is also interesting to examine the DD yield produced in the DT gas-filled CH Symcaps (the TT spectrum overwhelms the DD yield in pure T_2 filled Symcaps). This comparison can help

confirm the assumptions of Eqs. 6-7, especially in the context of previous studies, which have shown some anomalous yield behavior that would complicate the interpretation of the data.⁴⁹⁻⁵¹ These previous anomalous observations have been hypothesized to be caused by fuel isotope species separation⁵² or plasma kinetic effects,⁵³ both of which are predicted to vanish at the higher density and lower temperatures utilized in the NIF Symcap platform because of much higher ion-ion collisionality.

The DD reaction has two branches, but only the neutron branch is observable due to the high total ρR of the fuel and shell at bang-time. The neutron branch is described by:



The DD neutron yield ratio to the DT neutron yield ratio is plotted in Figure 12 as a function the predicted ratio using the observed ion temperature. The predicted ratio also considers the initial fuel ratio and an approximate attenuation correction for the escaping DD and DT neutron through the compressed shell material. Figure 12 shows that the neutron yield ratio is well understood and helps confirm the expectation that anomalous kinetic or species separation effects are not important in these experiments.

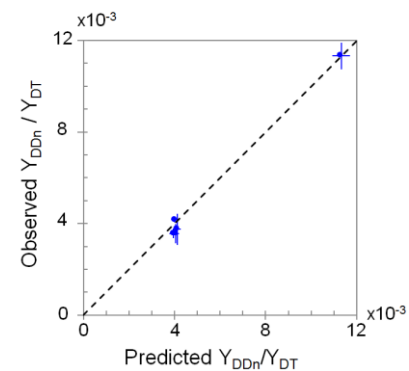


Figure 12: The observed DD neutron yield to DT neutron yield ratio (Y_{DDn} / Y_{DT}) as a function of the predicted yield ratio, when using the measured DT ion temperature and accounting for neutron attenuation, for five DT Symcap implosions.

C. Observed DT neutron and TT neutron bang-times

The particle-time-of-flight (pTOF) diagnostic⁵⁴ was used to measure the nuclear DT and TT bang-times. The pTOF observes the time-dependent neutron emission from the capsule using a W filtered, 200 μm thick CVD-diamond, placed 50 cm from the implosion. Figure 13a shows the recorded pTOF signal history from a CH TT Symcap showing a sharp rise at ~ 33 ns corresponding to the 14 MeV DT neutron emission and a second rise at 35 ns corresponding to the high energy edge of the TT neutron spectrum at 9.44 MeV. A best fit to the DT neutron spectrum (indicated as the red dashed curve) is used to obtain a DT bang-time of 22.45 ± 0.05 ns, after correcting for the neutron time of flight and pTOF detector response. The rising edge of the TTn spectrum was also used to infer the TT neutron bang-time of 22.52 ± 0.06 ns. The DT and TT bang-times are in agreement, as expected, since they both are produced in the gas-core for the CH

TT Symcap. Figure 13b shows the pTOF signal for a CD Symcap. The DT bang-time was measured to be 22.53 ± 0.05 ns, which is the time of peak D and T mix-induced neutron emission in the CD Symcap. The TTn signal is overwhelmed by the significantly higher DT yield, when compared to the CH TT Symcap, making the TTn bang-time measurement more challenging.

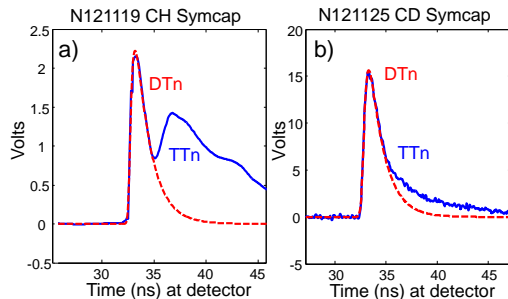


Figure 13: a) Observed pTOF data showing DT and TT neutron signals from a TT CH Symcap. A best fit to the DT neutron burn is indicated by the red dashed curve, which is used to obtain the time of peak core DTn and TTn emission. b) Observed pTOF data showing DT and TT signals from a CD Symcap. A best fit to the DT neutron burn is indicated by the red dashed curve, which is used to obtain the time of peak mix-induced DTn emission.

D. X-ray core imaging

The hotspot shape was observed using time-gated X-ray framing cameras that are configured for the hot-spot self-emission ($h\nu > 6$ keV). These measurements, performed with the GXD and hGXD instruments using a spatial resolution of ~ 10 μm and a temporal resolution of ~ 100 ps,^{55, 56} show that hotspot shape implodes into a $55\text{-}60$ μm radius hotspot with a typically prolate shape (see Table 1). The X-ray bang-time obtained from the framing camera images is 22.5 ns for this platform in good agreement with the x-ray diamond detectors in the south pole (SPBT)⁵⁷ and the x-ray streak camera in the north pole (SPIDER).⁵⁸ In addition, the x-ray bang-time is in good agreement with the nuclear bang-time from the pTOF diagnostic described earlier.⁵⁴ Interestingly, these X-ray images also show brightly radiating objects traversing through the hotspot, as shown in Figure 14. These bright spot features are common to implosions in this campaign, partly due to the fact that the tritium fill radiates less than previous D^3He Symcaps, accentuating higher Z emission from hot shell material. These objects have velocities that approach $\sim 100\text{-}150$ km/s. Common to all implosions on this platform, these objects may be tips of fingers or chunks of ablator, developed from instability growth, piercing and cooling the hotspot. A schematic of the orientation of the fill tube to both the equatorial and polar image frames is shown. Often, at least one object appears correlated to the fill tube orientation, implying that a jet seeded by the fill tube is injecting brightly radiating CH into the hotspot.^{59, 60} The exact origin, the performance impact, and the role of these features in bringing mix into the hotspot is an area of active investigation.

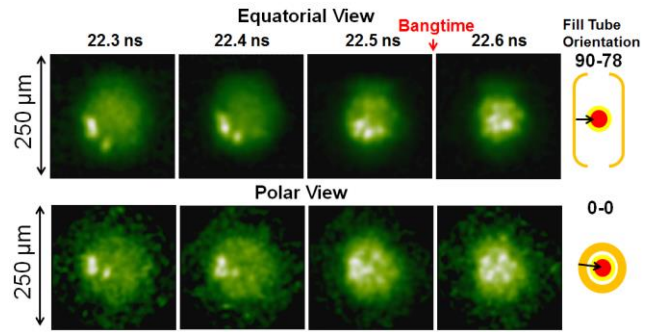


Figure 14: Time gated self-emission x-ray images of shot N130315 from an equatorial view obtained with the hGXD instrument, and the polar view (viewing into laser entrance hole) obtained from the GXD instrument. Several bright spots of radiating plastic chunks are observed traversing the core near bang-time.

The neutron imaging system (NIS)⁶¹ was also used to image the TT core burn and DT mix burn regions simultaneously by time-gating two NIS CCD cameras, which are normally timed to look at DT and down-scattered neutrons. A method to infer mix mass from the difference in the sizes of the two burn regions is currently under development.⁶² Preliminary estimates are encouraging and seem consistent with the yield method described earlier.

IV. Summary and future work

An experimental methodology to study fuel and shell atomic scale mix at the NIF has been developed using tritium-gas filled CD Symcap implosions. Deuterium from the plastic shell mixing into the hot-spot creates an unambiguous signature of atomic scale mix by producing DT fusion neutrons with the hot tritium core. By taking advantage of the advanced NIF diagnostic suite, this platform measures the TT and DT neutron simultaneously, ion temperature, X-ray and neutron core imaging, along with X-ray and nuclear bang-times. The simultaneous measurements of TT and DT neutrons places strong constraints on simulations by obtaining both core performance and atomic gas-shell mix, independently. CD layers flush with the gas-shell interface and recessed to up to 8 μm have shown that most of the mix occurs at the inner shell surface. Ablation front instabilities may also play a role in the observed data and will be the topic of future efforts in simulation and experiments.

With this new and powerful mix platform now commissioned, experiments are being proposed to study a wide variety of topics. For example, increasing the implosion convergence closer to that of cryogenic DT experiments is now underway. The expectation is that this will further constrain hydrodynamic simulations and atomic-mix models, providing the opportunity for additional model development, while also being more relevant to DT-layered ignition experiments. Experiments that combine X-ray tracer measurements in Ge and Cu doped capsules with the CD layer are now also being designed. One such design would include a CD layer with mostly hydrogen fill and trace tritium along with Cu and Ge “tri-doping.” This would provide simulations and redundant measurements of chunk mix from DD neutron and Cu and Ge emission (Cu and Ge placed at

different ablator locations) with atomic-mix data from DT neutrons.^{63, 64} Also experiments to quantify the seeds and role of ablation front instabilities in injected shell material in the hotspot are being proposed. One experimental concept is to simply repeat the 8 μm recessed shot N130614 so that inner 8 μm of the shell is CH but with the CD extending all the way from 8 μm recessed through the thickness of the shell (instead of 4 μm thick). If significant material is injected into the core via ablation front growth, the DT yield will be correspondingly higher than N130614. Another proposal is to directly measure plastic mix in cryogenic experiments, using a deuterated plastic ablator with a pure hydrogen-tritium-layer. Experiments are also proposed to study ablation front mix using ^{12}C tracer layers probed with the $^{12}\text{C}(\text{n},\text{n}')\gamma$ reaction in ^{13}CH shells⁶⁵ using the gamma reaction history diagnostic.⁶⁶ Other drives, such as the “high foot”,⁶⁷ with dramatically different ablation front and deceleration phase growth, are also being proposed for experiments in the CD Symcap platform. Developing benchmarked mix models capable of designing targets robust to the deleterious performance losses due to mix is the ultimate goal of this campaign.

This work was performed under the auspices of the U.S. Department of Energy by Lawrence Livermore National Laboratory under Contract DE-AC52-07NA27344.

V. References

1. J. A. Paisner, E. M. Campbell, and W. J. Hogan, *Fusion Technol.* **26**, 755 (1994).
2. G. H. Miller, E. I. Moses and C. R. Wuest, *Opt. Eng.* **43** (12), 2841-2853 (2004).
3. E. I. Moses, *Journal of Physics: Conference Series* **112** (1), 012003 (2008).
4. S. W. Haan, J. D. Lindl, D. A. Callahan, D. S. Clark, J. D. Salmonson, B. A. Hammel, L. J. Atherton, R. C. Cook, M. J. Edwards, S. Glenzer, A. V. Hamza, S. P. Hatchett, M. C. Herrmann, D. E. Hinkel, D. D. Ho, H. Huang, O. S. Jones, J. Kline, G. Kyrala, O. L. Landen, B. J. MacGowan, M. M. Marinak, D. D. Meyerhofer, J. L. Milovich, K. A. Moreno, E. I. Moses, D. H. Munro, A. Nikroo, R. E. Olson, K. Peterson, S. M. Pollaine, J. E. Ralph, H. F. Robey, B. K. Spears, P. T. Springer, L. J. Suter, C. A. Thomas, R. P. Town, R. Vesey, S. V. Weber, H. L. Wilkens and D. C. Wilson, *Physics of Plasmas* **18** (5), 051001 (2011).
5. J. D. Lindl, P. Amendt, R. L. Berger, S. G. Glendinning, S. H. Glenzer, S. W. Haan, R. L. Kauffman, O. L. Landen and L. J. Suter, *Physics of Plasmas* **11**, 339 (2004).
6. S. H. Glenzer, D. A. Callahan, A. J. MacKinnon, J. L. Kline, G. Grim, E. T. Alger, R. L. Berger, L. A. Bernstein, R. Betti, D. L. Bleuel, T. R. Boehly, D. K. Bradley, S. C. Burkhardt, R. Burr, J. A. Caggiano, C. Castro, D. T. Casey, C. Choate, D. S. Clark, P. Celliers, C. J. Cerjan, G. W. Collins, E. L. Dewald, P. DiNicola, J. M. DiNicola, L. Divol, S. Dixit, T. Doppner, R. Dylla-Spears, E. Dzenitis, M. Eckart, G. Erbert, D. Farley, J. Fair, D. Fittinghoff, M. Frank, L. J. A. Frenje, S. Friedrich, M. G. Johnson, C. Gibson, E. Giraldez, V. Glebov, S. Glenn, N. Guler, S. W. Haan, B. J. Haid, B. A. Hammel, A. V. Hamza, C. A. Haynam, G. M. Heestand, M. Hermann, H. W. Hermann, D. G. Hicks, D. E. Hinkel, J. P. Holder, D. M. Holunda, J. B. Horner, W. W. Hsing, H. Huang, N. Izumi, M. Jackson, O. S. Jones, D. H. Kalantar, R. Kauffman, J. D. Kilkenny, R. K. Kirkwood, J. Klingmann, T. Kohut, J. P. Knauer, J. A. Koch, B. Kozioziemki, G. A. Kyrala, A. L. Kritch, J. Kroll, K. L. Fortune, L. Lagin, O. L. Landen, D. W. Larson, D. LaTray, R. J. Leeper, S. L. Pape, J. D. Lindl, R. Lowe-Webb, T. Ma, J. McNaney, A. G. MacPhee, T. N. Malsbury, E. Mapoles, C. D. Marshall, N. B. Meezan, F. Merrill, P. Michel, J. D. Moody, A. S. Moore, M. Moran, K. A. Moreno, D. H. Munro, B. R. Nathan, A. Nikroo, R. E. Olson, C. D. Orth, A. E. Pak, P. K. Patel, T. Parham, R. Petrasso, J. E. Ralph, H. Rinderknecht, S. P. Regan, H. F. Robey, J. S. Ross, M. D. Rosen, R. Sacks, J. D. Salmonson, R. Saunders, J. Sater, C. Sangster, M. B. Schneider, F. H. Seguin, M. J. Shaw, B. K. Spears, P. T. Springer, W. Stoeffl, L. J. Suter, C. A. Thomas, R. Tommasini, R. P. J. Town, C. Walters, S. Weaver, S. V. Weber, P. J. Wegner, P. K. Whitman, K. Widmann, C. C. Widmayer, C. H. Wilde, D. C. Wilson, B. V. Wontershem, B. J. MacGowan, L. J. Atherton, M. J. Edwards and E. I. Moses, *Physics of Plasmas* **19** (5), 056318 (2012).
7. M. J. Edwards, P. K. Patel, J. D. Lindl, L. J. Atherton, S. H. Glenzer, S. W. Haan, J. D. Kilkenny, O. L. Landen, E. I. Moses, A. Nikroo, R. Petrasso, T. C. Sangster, P. T. Springer, S. Batha, R. Benedetti, L. Bernstein, R. Betti, D. L. Bleuel, T. R. Boehly, D. K. Bradley, J. A. Caggiano, D. A. Callahan, P. M. Celliers, C. J. Cerjan, K. C. Chen, D. S. Clark, G. W. Collins, E. L. Dewald, L. Divol, S. Dixit, T. Doeppner, D. H. Edgell, J. E. Fair, M. Farrell, R. J. Fortner, J. Frenje, M. G. G. Johnson, E. Giraldez, V. Y. Glebov, G. Grim, B. A. Hammel, A. V. Hamza, D. R. Harding, S. P. Hatchett, N. Hein, H. W. Herrmann, D. Hicks, D. E. Hinkel, M. Hoppe, W. W. Hsing, N. Izumi, B. Jacoby, O. S. Jones, D. Kalantar, R. Kauffman, J. L. Kline, J. P. Knauer, J. A. Koch, B. J. Kozioziemski, G. Kyrala, K. N. LaFortune, S. L. Pape, R. J. Leeper, R. Lerche, T. Ma, B. J. MacGowan, A. J. MacKinnon, A. Macphee, E. R. Mapoles, M. M. Marinak, M. Mauldin, P. W. McKenty, M. Meezan, P. A. Michel, J. Milovich, J. D. Moody, M. Moran, D. H. Munro, C. L. Olson, K. Opachich, A. E. Pak, T. Parham, H.-S. Park, J. E. Ralph, S. P. Regan, B. Remington, H. Rinderknecht, H. F. Robey, M. Rosen, S. Ross, J. D. Salmonson, J. Sater, D. H. Schneider, F. H. Seguin, S. M. Sepke, D. A. Shaughnessy, V. A. Smalyuk, B. K. Spears, C. Stoeckl, W. Stoeffl, L. Suter, C. A. Thomas, R. Tommasini, R. P. Town, S. V. Weber, P. J. Wegner, K. Widman, M. Wilke, D. C. Wilson, C. B. Yeamans and A. Zylstra, *Physics of Plasmas* **20** (7), 070501 (2013).
8. S. P. Regan, R. Epstein, B. A. Hammel, L. J. Suter, J. Ralph, H. Scott, M. A. Barrios, D. K. Bradley, D. A. Callahan, C. Cerjan, G. W. Collins, S. N. Dixit, T. Doeppner, M. J. Edwards, D. R. Farley, S. Glenn, S. H. Glenzer, I. E. Golovkin, S. W. Haan, A. Hamza, D. G. Hicks, N. Izumi, J. D. Kilkenny, J. L. Kline, G. A. Kyrala, O. L. Landen, T. Ma, J. J. MacFarlane, R. C. Mancini, R. L. McCrory, N. B. Meezan, D. D. Meyerhofer, A. Nikroo, K. J. Peterson, T. C. Sangster, P. Springer and R. P. J. Town, *Physics of Plasmas* **19** (5), 056307 (2012).
9. T. Ma, P. K. Patel, N. Izumi, P. T. Springer, M. H. Key, L. J. Atherton, L. R. Benedetti, D. K. Bradley, D. A. Callahan, P. M. Celliers, C. J. Cerjan, D. S. Clark, E. L. Dewald, S. N. Dixit, T. Döppner, D. H. Edgell, R. Epstein, S. Glenn, G. Grim, S. W. Haan, B. A. Hammel, D. Hicks, W. W. Hsing, O. S. Jones, S. F. Khan, J. D. Kilkenny, J. L. Kline, G. A. Kyrala, O. L. Landen, S. Le Pape, B. J. MacGowan, A. J. Mackinnon, A. G. MacPhee, N. B. Meezan, J. D. Moody, A. Pak, T. Parham, H. S. Park, J. E. Ralph, S. P. Regan, B. A. Remington, H. F. Robey, J. S. Ross, B. K. Spears, V. Smalyuk, L. J. Suter, R. Tommasini, R. P. Town, S. V. Weber, J. D. Lindl, M. J. Edwards, S. H. Glenzer and E. I. Moses, *Physical Review Letters* **111** (8), 085004 (2013).

10. V. A. Smalyuk, D. T. Casey, D. S. Clark, M. J. Edwards, S. W. Haan, A. Hamza, D. E. Hoover, W. W. Hsing, O. Hurricane, J. D. Kilkenny, J. Kroll, O. L. Landen, A. Moore, A. Nikroo, L. Peterson, K. Raman, B. A. Remington, H. F. Robey, S. V. Weber and K. Widmann, *Physical Review Letters* **112** (18), 185003 (2014).
11. V. A. Smalyuk, R. E. Tipton, J. E. Pino, D. T. Casey, G. P. Grim, B. A. Remington, D. P. Rowley, S. V. Weber, M. Barrios, L. R. Benedetti, D. L. Bleuel, D. K. Bradley, J. A. Caggiano, D. A. Callahan, C. J. Cerjan, D. S. Clark, D. H. Edgell, M. J. Edwards, J. A. Frenje, M. Gatou-Johnson, V. Y. Glebov, S. Glenn, S. W. Haan, A. Hamza, R. Hatarik, W. W. Hsing, N. Izumi, S. Khan, J. D. Kilkenny, J. Kline, J. Knauer, O. L. Landen, T. Ma, J. M. McNaney, M. Mintz, A. Moore, A. Nikroo, A. Pak, T. Parham, R. Petrasso, D. B. Sayre, M. B. Schneider, R. Tommasini, R. P. Town, K. Widmann, D. C. Wilson and C. B. Yeamans, *Physical Review Letters* **112** (2), 025002 (2014).
12. O. L. Landen, T. R. Boehly, D. K. Bradley, D. G. Braun, D. A. Callahan, P. M. Celliers, G. W. Collins, E. L. Dewald, L. Divol, S. H. Glenzer, A. Hamza, D. G. Hicks, N. Hoffman, N. Izumi, O. S. Jones, R. K. Kirkwood, G. A. Kyrala, P. Michel, J. Milovich, D. H. Munro, A. Nikroo, R. E. Olson, H. F. Robey, B. K. Spears, C. A. Thomas, S. V. Weber, D. C. Wilson, M. M. Marinak, L. J. Suter, B. A. Hammel, D. D. Meyerhofer, J. Atherton, J. Edwards, S. W. Haan, J. D. Lindl, B. J. MacGowan and E. I. Moses, *Physics of Plasmas* **17** (5), 056301-056308 (2010).
13. D. C. Wilson, P. S. Ebey, T. C. Sangster, W. T. Shmayda, V. Y. Glebov and R. A. Lerche, *Physics of Plasmas* **18** (11), 112707 (2011).
14. J. R. Rygg, J. A. Frenje, C. K. Li, F. H. Séguin, R. D. Petrasso, J. A. Delettrez, V. Y. Glebov, V. N. Goncharov, D. D. Meyerhofer, P. B. Radha, S. P. Regan and T. C. Sangster, *Physics of Plasmas* **14** (5), 056306 (2007).
15. J. R. Rygg, J. A. Frenje, C. K. Li, F. H. Séguin, R. D. Petrasso, V. Y. Glebov, D. D. Meyerhofer, T. C. Sangster and C. Stoeckl, *Physical Review Letters* **98** (21), 215002 (2007).
16. H. G. Rinderknecht et. al., accepted for publication *Phys. Rev. Lett.*
17. T. R. Boehly, D. L. Brown, R. S. Craxton, R. L. Keck, J. P. Knauer, J. H. Kelly, T. J. Kessler, S. A. Kumpan, S. J. Loucks, S. A. Letzring, F. J. Marshall, R. L. McCrory, S. F. B. Morse, W. Seka, J. M. Soures and C. P. Verdon, *Optics Communications* **133** (1-6), 495-506 (1997).
18. J. D. Moody, P. Michel, L. Divol, R. L. Berger, E. Bond, D. K. Bradley, D. A. Callahan, E. L. Dewald, S. Dixit, M. J. Edwards, S. Glenn, A. Hamza, C. Haynam, D. E. Hinkel, N. Izumi, O. Jones, J. D. Kilkenny, R. K. Kirkwood, J. L. Kline, W. L. Kruer, G. A. Kyrala, O. L. Landen, S. LePape, J. D. Lindl, B. J. MacGowan, N. B. Meezan, A. Nikroo, M. D. Rosen, M. B. Schneider, D. J. Strozzi, L. J. Suter, C. A. Thomas, R. P. J. Town, K. Widmann, E. A. Williams, L. J. Atherton, S. H. Glenzer and E. I. Moses, *Nat Phys* **8** (4), 344-349 (2012).
19. D. S. Clark, S. W. Haan, B. A. Hammel, J. D. Salmonson, D. A. Callahan and R. P. J. Town, *Physics of Plasmas* **17** (5), 052703 (2010).
20. A. Nikroo, K. C. Chen, M. L. Hoppe, H. Huang, J. R. Wall, H. Xu, M. W. McElfresh, C. S. Alford, R. C. Cook, J. C. Cooley, R. Fields, R. Hackenberg, R. P. Doerner and M. Baldwin, *Physics of Plasmas* **13** (5), 056302 (2006).
21. G. A. Kyrala, S. Dixit, S. Glenzer, D. Kalantar, D. Bradley, N. Izumi, N. Meezan, O. L. Landen, D. Callahan, S. V. Weber, J. P. Holder, S. Glenn, M. J. Edwards, P. Bell, J. Kimbrough, J. Koch, R. Prasad, L. Suter, J. L. Kline and J. Kilkenny, *Review of Scientific Instruments* **81** (10), - (2010).
22. R. M. Darlington, T. L. McAbee and G. Rodrigue, *Computer Physics Communications* **135** (1), 58-73 (2001).
23. R. E. Tipton (private communication).
24. G. Dimonte and R. Tipton, *Physics of Fluids* **18** (8), 085101 (2006).
25. J. Pino, to be published.
26. D. S. Clark, S. W. Haan, A. W. Cook, M. J. Edwards, B. A. Hammel, J. M. Koning and M. M. Marinak, *Physics of Plasmas* **18** (8), 082701 (2011).
27. S. Atzeni and J. Meyer-ter-Vehn, *The physics of inertial fusion*. (Oxford University Press, Oxford, 2004).
28. M. B. Chadwick, P. Óblozinský, M. Herman, N. M. Greene, R. D. McKnight, D. L. Smith, P. G. Young, R. E. MacFarlane, G. M. Hale, S. C. Frankle, A. C. Kahler, T. Kawano, R. C. Little, D. G. Madland, P. Moller, R. D. Mosteller, P. R. Page, P. Talou, H. Trellue, M. C. White, W. B. Wilson, R. Arcilla, C. L. Dunford, S. F. Mughabghab, B. Pritychenko, D. Rochman, A. A. Sonzogni, C. R. Lubitz, T. H. Trumbull, J. P. Weinman, D. A. Brown, D. E. Cullen, D. P. Heinrichs, D. P. McNabb, H. Derrien, M. E. Dunn, N. M. Larson, L. C. Leal, A. D. Carlson, R. C. Block, J. B. Briggs, E. T. Cheng, H. C. Huria, M. L. Zerkle, K. S. Kozier, A. Courcelle, V. Pronyaev and S. C. van der Marck, *Nuclear Data Sheets* **107** (12), 2931-3060 (2006).
29. H. S. Bosch and G. M. Hale, *Nuclear Fusion* **32** (4), 611 (1992).
30. V. I. Serov, S. N. Abramovich and L. A. Morkin, *Atomic Energy* **42** (1), 66-69 (1977).
31. R. E. Brown and N. Jarmie, *Radiation Effects* **92** (1), 45 - 57 (1986).
32. R. J. Slobodrian, *Reports on Progress in Physics* **34** (1), 175 (1971).
33. I. J. Thompson and S. Quaglioni (private communication).
34. C. Wong, J. D. Anderson and J. W. McClure, *Nuclear Physics* **71** (1), 106-112 (1965).
35. K. W. Allen, E. Almqvist, J. T. Dewan, T. P. Pepper and J. H. Sanders, *Phys Rev* **82** (2), 262 (1951).
36. S. J. Bame and W. T. Leland, *Phys Rev* **106** (6), 1257 (1957).
37. D. T. Casey, J. A. Frenje, M. Gatou Johnson, M. J. E. Manuel, N. Sinenian, A. B. Zylstra, F. H. Séguin, C. K. Li, R. D. Petrasso, V. Y. Glebov, P. B. Radha, D. D. Meyerhofer, T. C. Sangster, D. P. McNabb, P. A. Amendt, R. N. Boyd, S. P. Hatchett, S. Quaglioni, J. R. Rygg, I. J. Thompson, A. D. Bacher, H. W. Herrmann and Y. H. Kim, *Physical Review Letters* **109** (2), 025003 (2012).
38. D. B. Sayre, C. R. Brune, J. A. Caggiano, V. Y. Glebov, R. Hatarik, A. D. Bacher, D. L. Bleuel, D. T. Casey, C. J. Cerjan, M. J. Eckart, R. J. Fortner, J. A. Frenje, S. Friedrich, M. Gatou-Johnson, G. P. Grim, C. Hagmann, J. P. Knauer, J. L. Kline, D. P. McNabb, J. M. McNaney, J. M. Mintz, M. J. Moran, A. Nikroo, T. Phillips, J. E. Pino, B. A. Remington, D. P. Rowley, D. H. Schneider, V. A. Smalyuk, W. Stoeffl, R. E. Tipton, S. V. Weber and C. B. Yeamans, *Physical Review Letters* **111** (5), 052501 (2013).
39. C. B. Yeamans, D. L. Bleuel and L. A. Bernstein, *Review of Scientific Instruments* **83** (10), 10D315 (2012).
40. R. A. Lerche, V. Y. Glebov, M. J. Moran, J. M. McNaney, J. D. Kilkenny, M. J. Eckart, R. A. Zacharias, J. J.

- Haslam, T. J. Clancy, M. F. Yeoman, D. P. Warwas, T. C. Sangster, C. Stoeckl, J. P. Knauer and C. J. Horsfield, Review of Scientific Instruments **81** (10), 10D319 (2010).
41. V. Y. Glebov, T. C. Sangster, C. Stoeckl, J. P. Knauer, W. Theobald, K. L. Marshall, M. J. Shoup, III, T. Buczak, M. Cruz, T. Duffy, M. Romanofsky, M. Fox, A. Pruyne, M. J. Moran, R. A. Lerche, J. McNaney, J. D. Kilkenny, M. J. Eckart, D. Schneider, D. Munro, W. Stoeffl, R. Zacharias, J. J. Haslam, T. Clancy, M. Yeoman, D. Warwas, C. J. Horsfield, J. L. Bourgade, O. Landoas, L. Disdier, G. A. Chandler and R. J. Leeper, Review of Scientific Instruments **81** (10), 10D325-326 (2010).
42. M. G. Johnson, J. A. Frenje, D. T. Casey, C. K. Li, F. H. Seguin, R. Petrasso, R. Ashabrunner, R. M. Bionta, D. L. Bleuel, E. J. Bond, J. A. Caggiano, A. Carpenter, C. J. Cerjan, T. J. Clancy, T. Doeppner, M. J. Eckart, M. J. Edwards, S. Friedrich, S. H. Glenzer, S. W. Haan, E. P. Hartouni, R. Hatarik, S. P. Hatchett, O. S. Jones, G. Kyrala, S. L. Pape, R. A. Lerche, O. L. Landen, T. Ma, A. J. MacKinnon, M. A. McKernan, M. J. Moran, E. Moses, D. H. Munro, J. McNaney, H. S. Park, J. Ralph, B. Remington, J. R. Rygg, S. M. Sepke, V. Smalyuk, B. Spears, P. T. Springer, C. B. Yeamans, M. Farrell, D. Jasion, J. D. Kilkenny, A. Nikroo, R. Paguio, J. P. Knauer, V. Y. Glebov, T. C. Sangster, R. Betti, C. Stoeckl, J. Magoon, M. J. Shoup, III, G. P. Grim, J. Kline, G. L. Morgan, T. J. Murphy, R. J. Leeper, C. L. Ruiz, G. W. Cooper and A. J. Nelson, Review of Scientific Instruments **83** (10), 10D308 (2012).
43. D. T. Casey, J. A. Frenje, M. G. Johnson, F. H. Seguin, C. K. Li, R. D. Petrasso, V. Y. Glebov, J. Katz, J. Magoon, D. D. Meyerhofer, T. C. Sangster, M. J. Shoup, J. Ulreich, R. C. Ashabrunner, R. M. Bionta, A. C. Carpenter, B. Felker, H. Y. Khater, S. LePape, A. MacKinnon, M. A. McKernan, M. Moran, J. R. Rygg, M. F. Yeoman, R. Zacharias, R. J. Leeper, K. Fletcher, M. Farrell, D. Jasion, J. Kilkenny and R. Paguio, Review of Scientific Instruments **84** (4), 043506 (2013).
44. J. A. Frenje, R. Bionta, E. J. Bond, J. A. Caggiano, D. T. Casey, C. Cerjan, J. Edwards, M. Eckart, D. N. Fittinghoff, S. Friedrich, V. Y. Glebov, S. Glenzer, G. Grim, S. Haan, R. Hatarik, S. Hatchett, M. G. Johnson, O. S. Jones, J. D. Kilkenny, J. P. Knauer, O. Landen, R. Leeper, S. L. Pape, R. Lerche, C. K. Li, A. Mackinnon, J. McNaney, F. E. Merrill, M. Moran, D. H. Munro, T. J. Murphy, R. D. Petrasso, R. Rygg, T. C. Sangster, F. H. Séguin, S. Sepke, B. Spears, P. Springer, C. Stoeckl and D. C. Wilson, Nuclear Fusion **53** (4), 043014 (2013).
45. J. Caggiano, to be published.
46. B. K. Spears, S. Glenzer, M. J. Edwards, S. Brandon, D. Clark, R. Town, C. Cerjan, R. Dylla-Spears, E. Mapoles, D. Munro, J. Salmonson, S. Sepke, S. Weber, S. Hatchett, S. Haan, P. Springer, E. Moses, J. Kline, G. Kyrala and D. Wilson, Physics of Plasmas **19** (5), 056316 (2012).
47. A. J. Mackinnon, J. L. Kline, S. N. Dixit, S. H. Glenzer, M. J. Edwards, D. A. Callahan, N. B. Meezan, S. W. Haan, J. D. Kilkenny, T. Döppner, D. R. Farley, J. D. Moody, J. E. Ralph, B. J. MacGowan, O. L. Landen, H. F. Robey, T. R. Boehly, P. M. Celliers, J. H. Eggert, K. Krauter, G. Frieders, G. F. Ross, D. G. Hicks, R. E. Olson, S. V. Weber, B. K. Spears, J. D. Salmonson, P. Michel, L. Divol, B. Hammel, C. A. Thomas, D. S. Clark, O. S. Jones, P. T. Springer, C. J. Cerjan, G. W. Collins, V. Y. Glebov, J. P. Knauer, C. Sangster, C. Stoeckl, P. McKenty, J. M. McNaney, R. J. Leeper, C. L. Ruiz, G. W. Cooper, A. G. Nelson, G. G. A. Chandler, K. D. Hahn, M. J. Moran, M. B. Schneider, N. E. Palmer, R. M. Bionta, E. P. Hartouni, S. LePape, P. K. Patel, N. Izumi, R. Tommasini, E. J. Bond, J. A. Caggiano, R. Hatarik, G. P. Grim, F. E. Merrill, D. N. Fittinghoff, N. Guler, O. Drury, D. C. Wilson, H. W. Herrmann, W. Stoeffl, D. T. Casey, M. G. Johnson, J. A. Frenje, R. D. Petrasso, A. Zylestra, H. Rinderknecht, D. H. Kalantar, J. M. Dzenitis, P. Di Nicola, D. C. Eder, W. H. Courdin, G. Gururangan, S. C. Burkhardt, S. Friedrich, D. L. Blueuel, I. A. Bernstein, M. J. Eckart, D. H. Munro, S. P. Hatchett, A. G. Macphee, D. H. Edgett, D. K. Bradley, P. M. Bell, S. M. Glenn, N. Simanovskia, M. A. Barrios, R. Benedetti, G. A. Kyrala, R. P. J. Town, E. L. Dewald, J. L. Milovich, K. Widmann, A. S. Moore, G. LaCaille, S. P. Regan, L. J. Suter, B. Felker, R. C. Ashabrunner, M. C. Jackson, R. Prasad, M. J. Richardson, T. R. Kohut, P. S. Datte, G. W. Krauter, J. J. Klingman, R. F. Burr, T. A. Land, M. R. Hermann, D. A. Latray, R. L. Saunders, S. Weaver, S. J. Cohen, L. Berzins, S. G. Brass, E. S. Palma, R. R. Lowe-Webb, G. N. McHalle, P. A. Arnold, L. J. Lagin, C. D. Marshall, G. K. Brunton, D. G. Mathisen, R. D. Wood, J. R. Cox, R. B. Ehrlich, K. M. Knittel, M. W. Bowers, R. A. Zacharias, B. K. Young, J. P. Holder, J. R. Kimbrough, T. Ma, K. N. La Fortune, C. C. Widmayer, M. J. Shaw, G. V. Erbert, K. S. Jancaitis, J. M. DiNicola, C. Orth, G. Heestand, R. Kirkwood, C. Haynam, P. J. Wegner, P. K. Whitman, A. Hamza, E. G. Dzenitis, R. J. Wallace, S. D. Bhandarkar, T. G. Parham, R. Dylla-Spears, E. R. Mapoles, B. J. Kozioziemski, J. D. Sater, C. F. Walters, B. J. Haid, J. Fair, A. Nikroo, E. Giraldez, K. Moreno, B. Vanwonterghem, R. L. Kauffman, S. Batha, D. W. Larson, R. J. Fortner, D. H. Schneider, J. D. Lindl, R. W. Patterson, L. J. Atherton and E. I. Moses, Physical Review Letters **108** (21), 215005 (2012).
48. If the CD pressure cannot be neglected then an analytic estimate of the mix mass becomes more challenging because a measure of the volume of the mix region is required.
49. J. R. Rygg, J. A. Frenje, C. K. Li, F. H. Seguin, R. D. Petrasso, J. A. Delettrez, V. Y. Glebov, V. N. Goncharov, D. D. Meyerhofer, S. P. Regan, T. C. Sangster and C. Stoeckl, Physics of Plasmas **13** (5), 052702 (2006).
50. H. W. Herrmann, J. R. Langenbrunner, J. M. Mack, J. H. Cooley, D. C. Wilson, S. C. Evans, T. J. Sedillo, G. A. Kyrala, S. E. Caldwell, C. S. Young, A. Nobile, J. Wermer, S. Paglieri, A. M. McEvoy, Y. Kim, S. H. Batha, C. J. Horsfield, D. Drew, W. Garbett, M. Rubery, V. Y. Glebov, S. Roberts and J. A. Frenje, Physics of Plasmas **16** (5), 056312 (2009).
51. D. T. Casey, J. A. Frenje, M. Gatun Johnson, M. J. E. Manuel, H. G. Rinderknecht, N. Sinenian, F. H. Séguin, C. K. Li, R. D. Petrasso, P. B. Radha, J. A. Delettrez, V. Y. Glebov, D. D. Meyerhofer, T. C. Sangster, D. P. McNabb, P. A. Amendt, R. N. Boyd, J. R. Rygg, H. W. Herrmann, Y. H. Kim and A. D. Bacher, Physical Review Letters **108** (7), 075002 (2012).
52. P. Amendt, S. C. Wilks, C. Bellei, C. K. Li and R. D. Petrasso, Physics of Plasmas **18** (5), 056308 (2011).
53. K. Molvig, N. M. Hoffman, B. J. Albright, E. M. Nelson and R. B. Webster, Physical Review Letters **109** (9), 095001 (2012).
54. H. G. Rinderknecht, M. G. Johnson, A. B. Zylstra, N. Sinenian, M. J. Rosenberg, J. A. Frenje, C. J. Waugh, C. K. Li, F. H. Seguin, R. D. Petrasso, J. R. Rygg, J. R. Kimbrough, A. MacPhee, G. W. Collins, D. Hicks, A. Mackinnon, P. Bell, R. Bionta, T. Clancy, R. Zacharias, T. Döppner, H. S. Park, S. LePape, O. Landen, N. Meezan, E. I. Moses, V. U. Glebov, C. Stoeckl, T. C. Sangster, R. Olson, J. Kline and J. Kilkenny, Review of Scientific Instruments **83** (10), 10D902 (2012).

55. P. M. Bell, D. K. Bradley, J. D. Kilkenny, A. Conder, C. Cerjan, C. Hagmann, D. Hey, N. Izumi, J. Moody, A. Teruya, J. Celeste, J. Kimbrough, H. Khater, M. J. Eckart and J. Ayers, *Review of Scientific Instruments* **81** (10), 10E540 (2010).
56. S. M. Glenn, L. R. Benedetti, D. K. Bradley, B. A. Hammel, N. Izumi, S. F. Khan, G. A. Kyrala, T. Ma, J. L. Milovich, A. E. Pak, V. A. Smalyuk, R. Tommasini and R. P. Town, *Review of Scientific Instruments* **83** (10), 10E519 (2012).
57. D. H. Edgell, D. K. Bradley, E. J. Bond, S. Burns, D. A. Callahan, J. Celeste, M. J. Eckart, V. Y. Glebov, D. S. Hey, G. Lacaille, J. D. Kilkenny, J. Kimbrough, A. J. Mackinnon, J. Magoon, J. Parker, T. C. Sangster, M. J. Shoup, III, C. Stoeckl, T. Thomas and A. MacPhee, *Review of Scientific Instruments* **83** (10), 10E119 (2012).
58. S. F. Khan, P. M. Bell, D. K. Bradley, S. R. Burns, J. R. Celeste, L. S. Dauffy, M. J. Eckart, M. A. Gerhard, C. Hagmann, D. I. Headley, J. P. Holder, N. Izumi, M. C. Jones, J. W. Kellogg, H. Y. Khater, J. R. Kimbrough, A. G. Macphee, Y. P. Opachich, N. E. Palmer, R. B. Petre, J. L. Porter, R. T. Shelton, T. L. Thomas and J. B. Worden, 850505-850505 (2012).
59. S. H. Langer, N. Izumi, T. R. Dittrich and S. W. Haan, *High Energy Density Physics* **3** (1–2), 169–174 (2007).
60. M. A. Barrios, S. P. Regan, L. J. Suter, S. Glenn, L. R. Benedetti, D. K. Bradley, G. W. Collins, R. Epstein, B. A. Hammel, G. A. Kyrala, N. Izumi, T. Ma, H. Scott and V. A. Smalyuk, *Physics of Plasmas* **20** (7), 072706 (2013).
61. G. P. Grim, N. Guler, F. E. Merrill, G. L. Morgan, C. R. Danly, P. L. Volegov, C. H. Wilde, D. C. Wilson, D. S. Clark, D. E. Hinkel, O. S. Jones, K. S. Raman, N. Izumi, D. N. Fittinghoff, O. B. Drury, E. T. Alger, P. A. Arnold, R. C. Ashabrunner, L. J. Atherton, M. A. Barrios, S. Batha, P. M. Bell, L. R. Benedetti, R. L. Berger, L. A. Bernstein, L. V. Berzins, R. Betti, S. D. Bhandarkar, R. M. Bionta, D. L. Bleuel, T. R. Boehly, E. J. Bond, M. W. Bowers, D. K. Bradley, G. K. Brunton, R. A. Buckles, S. C. Burkhardt, R. F. Burr, J. A. Caggiano, D. A. Callahan, D. T. Casey, C. Castro, P. M. Celliers, C. J. Cerjan, G. A. Chandler, C. Choate, S. J. Cohen, G. W. Collins, G. W. Cooper, J. R. Cox, J. R. Cradick, P. S. Datte, E. L. Dewald, P. D. Nicola, J. M. D. Nicola, L. Divol, S. N. Dixit, R. Dylla-Spears, E. G. Dzenitis, M. J. Eckart, D. C. Eder, D. H. Edgell, M. J. Edwards, J. H. Eggert, R. B. Ehrlich, G. V. Erbert, J. Fair, D. R. Farley, B. Felker, R. J. Fortner, J. A. Frenje, G. Frieders, S. Friedrich, M. Gatu-Johnson, C. R. Gibson, E. Giraldez, V. Y. Glebov, S. M. Glenn, S. H. Glenzer, G. Gururangan, S. W. Haan, K. D. Hahn, B. A. Hammel, A. V. Hamza, E. P. Hartouni, R. Hatarik, S. P. Hatchett, C. Haynam, M. R. Hermann, H. W. Herrmann, D. G. Hicks, J. P. Holder, D. M. Holunga, J. B. Horner, W. W. Hsing, H. Huang, M. C. Jackson, K. S. Jancaitis, D. H. Kalantar, R. L. Kauffman, M. I. Kauffman, S. F. Khan, J. D. Kilkenny, J. R. Kimbrough, R. Kirkwood, J. L. Kline, J. P. Knauer, K. M. Knittel, J. A. Koch, T. R. Kohut, B. J. Kozioziemski, K. Krauter, G. W. Krauter, A. L. Kritcher, J. Kroll, G. A. Kyrala, K. N. L. Fortune, G. LaCaille, L. J. Lagin, T. A. Land, O. L. Landen, D. W. Larson, D. A. Latray, R. J. Leeper, T. L. Lewis, S. LePape, J. D. Lindl, R. R. Lowe-Webb, T. Ma, B. J. MacGowan, A. J. MacKinnon, A. G. MacPhee, R. M. Malone, T. N. Malsbury, E. Mapoles, C. D. Marshall, D. G. Mathisen, P. McKenty, J. M. McNaney, N. B. Meezan, P. Michel, J. L. Milovich, J. D. Moody, A. S. Moore, M. J. Moran, K. Moreno, E. I. Moses, D. H. Munro, B. R. Nathan, A. J. Nelson, A. Nikroo, R. E. Olson, C. Orth, A. E. Pak, E. S. Palma, T. G. Parham, P. K. Patel, R. W. Patterson, R. D. Petrasso, R. Prasad, J. E. Ralph, S. P. Regan, H. Rinderknecht, H. F. Robey, G. F. Ross, C. L. Ruiz, F. H. Seguin, J. D. Salmonson, T. C. Sangster, J. D. Sater, R. L. Saunders, M. B. Schneider, D. H. Schneider, M. J. Shaw, N. Simanovskaia, B. K. Spears, P. T. Springer, C. Stoeckl, W. Stoeffl, L. J. Suter, C. A. Thomas, R. Tommasini, R. P. Town, A. J. Traille, B. V. Wonteghem, R. J. Wallace, S. Weaver, S. V. Weber, P. J. Wegner, P. K. Whitman, K. Widmann, C. C. Widmayer, R. D. Wood, B. K. Young, R. A. Zacharias and A. Zylstra, *Physics of Plasmas* **20** (5), 056320 (2013).
62. G. Grim, to be published.
63. B. A. Hammel, H. A. Scott, S. P. Regan, C. Cerjan, D. S. Clark, M. J. Edwards, R. Epstein, S. H. Glenzer, S. W. Haan, N. Izumi, J. A. Koch, G. A. Kyrala, O. L. Landen, S. H. Langer, K. Peterson, V. A. Smalyuk, L. J. Suter and D. C. Wilson, *Physics of Plasmas* **18** (5), 056310 (2011).
64. S. P. Regan, R. Epstein, B. A. Hammel, L. J. Suter, H. A. Scott, M. A. Barrios, D. K. Bradley, D. A. Callahan, C. Cerjan, G. W. Collins, S. N. Dixit, T. Döppner, M. J. Edwards, D. R. Farley, K. B. Fournier, S. Glenn, S. H. Glenzer, I. E. Golovkin, S. W. Haan, A. Hamza, D. G. Hicks, N. Izumi, O. S. Jones, J. D. Kilkenny, J. L. Kline, G. A. Kyrala, O. L. Landen, T. Ma, J. J. MacFarlane, A. J. MacKinnon, R. C. Mancini, R. L. McCrory, N. B. Meezan, D. D. Meyerhofer, A. Nikroo, H. S. Park, J. Ralph, B. A. Remington, T. C. Sangster, V. A. Smalyuk, P. T. Springer and R. P. J. Town, *Physical Review Letters* **111** (4), 045001 (2013).
65. N. M. Hoffman, H. W. Herrmann, Y. H. Kim, H. H. Hsu, C. J. Horsfield, M. S. Rubery, E. K. Miller, E. Grafil, W. Stoeffl, J. A. Church, C. S. Young, J. M. Mack, D. C. Wilson, J. R. Langenbrunner, S. C. Evans, T. J. Sedillo, V. Y. Glebov and T. Duffy, *Physics of Plasmas (1994-present)* **20** (4), - (2013).
66. H. W. Herrmann, C. S. Young, J. M. Mack, Y. H. Kim, A. McEvoy, S. Evans, T. Sedillo, S. Batha, M. Schmitt, D. C. Wilson, J. R. Langenbrunner, R. Malone, M. I. Kaufman, B. C. Cox, B. Frogget, E. K. Miller, Z. A. Ali, T. W. Tunnell, W. Stoeffl, C. J. Horsfield and M. Rubery, *Journal of Physics: Conference Series* **244** (3), 032047 (2010).
67. O. A. Hurricane, D. A. Callahan, D. T. Casey, P. M. Celliers, C. Cerjan, E. L. Dewald, T. R. Dittrich, T. Doppner, D. E. Hinkel, L. F. B. Hopkins, J. L. Kline, S. Le Pape, T. Ma, A. G. MacPhee, J. L. Milovich, A. Pak, H. S. Park, P. K. Patel, B. A. Remington, J. D. Salmonson, P. T. Springer and R. Tommasini, *Nature* **506** (7488), 343–348 (2014).